Chalcogenide Letters

Tech Science Press

http://doi.org/10.32604/cl.2026.082364

ARTICLE

Design and Optimization of a Novel Double-Heterojunction Lead-Free Cs_2BiAgI_6 Perovskite Solar Cell with PCBM/C_{60} Bilayer ETL and CdTe HTL: Numerical Investigation

S. D. Al-Sahafi*

Department of Physics, Aljamoum University College, Umm Al-Qura University, Makkah, Saudi Arabia
*Corresponding Author: S. D. Al-Sahafi. Email: sdsahafi@uqu.edu.sa

Received: 14 March 2026; Accepted: 09 May 2026; Published: 02 June 2026

ABSTRACT: In this study, a lead-free double perovskite solar cell structure based on Cs_2BiAgI_6 was simulated and optimized to enhance photovoltaic performance. The device architecture follows the configuration: ITO/PCBM/C_{60}/Cs_2BiAgI_6/CdTe/Au. The thicknesses of the electron transport layer (ETL), absorber layer, and hole transport layer (HTL) are systematically optimized to evaluate their impact on key performance parameters. The results indicate that optimal performance is achieved with 600 nm thicknesses for all ETLs and HTL, and 2 μm for the Cs_2BiAgI_6 absorber. Under these conditions, the device exhibits a short-circuit current density of 23.23 mA/cm^2, an open-circuit voltage of 1.08 V, and a fill factor of 86.35%, resulting in a power conversion efficiency exceeding 22%. The improved performance is attributed to favorable energy band alignment and enhanced charge transport, which together facilitate efficient carrier extraction and reduce recombination losses. In addition, the device demonstrates a high quantum efficiency of approximately 96% within the 200–733 nm wavelength range. These findings highlight the promise of lead-free perovskite solar cells in delivering high performance while offering a more sustainable and environmentally friendly alternative to traditional lead-based technologies.

KEYWORDS: Lead-free perovskite; solar cells; bilayer ETL; renewables; photovoltaic; simulation

1 Introduction

Lead-free perovskite solar cells have recently gained significant interest as an alternative to conventional lead-based systems, primarily due to concerns related to toxicity and long-term environmental impact [1,2]. Among proposed candidates, double perovskites such as Cs_2BiAgI_6 have drawn particular attention. Their fully inorganic composition offers enhanced chemical and thermal stability, particularly under conditions where hybrid perovskites are prone to degradation, such as exposure to moisture and elevated temperatures [2,3]. This characteristic makes them particularly suitable for stable photovoltaic applications.

Despite these advantages, Cs_2BiAgI_6 and related lead-free double perovskites are still limited by intrinsic material properties. In particular, the presence of an indirect bandgap is typically associated with reduced optical absorption, which can limit overall device performance [3,4]. Consequently, improving efficiency cannot rely solely on the absorber layer; instead, careful design of the device architecture, especially the selection and optimization of charge-transport layers, is essential.

In this context, metal-oxide hole-transport layers (HTLs), including NiO, Cu_2O, and other wide-bandgap semiconductors, have been extensively investigated due to their chemical stability, favorable valence band

alignment, and relatively high hole mobility [2,5]. Compared to conventional organic HTLs, these materials offer improved durability and can effectively suppress recombination while enhancing charge extraction. It is widely recognized that proper selection and engineering of transport layers can significantly improve the performance of lead-free perovskite solar cells.

To address these challenges, the present work proposes a novel device architecture aimed at improving charge transport, reducing recombination, and enhancing overall performance. The absorber layer is based on Cs_2BiAgI_6, a lead-free double perovskite that has recently attracted attention for its stability and potential for photovoltaic applications.

Although Cs_2BiAgI_6 offers clear advantages in terms of stability and environmental compatibility, its indirect bandgap and moderate absorption require careful device-level optimization. In particular, the absorber thickness and transport layer design must be carefully tuned to achieve efficient carrier generation and collection.

The proposed architecture also incorporates CdTe (Cadmium Telluride), a well-established material in thin-film solar technology [6,7]. While CdTe is traditionally used as an absorber, its favorable electronic properties, including suitable band alignment and good hole transport characteristics, make it a viable candidate for use as a hole-transport layer in the present configuration. CdTe has demonstrated high efficiency and technological maturity, which further supports its integration into advanced device architectures [8–11]. Additionally, recent studies have explored light-trapping strategies to further enhance CdTe-based device performance [7].

For electron transport, a bilayer structure consisting of PCBM (Phenyl-C_{61}-butyric acid methyl ester) and C_{60} is employed. PCBM is widely used to facilitate efficient charge separation at interfaces, while C_{60} provides excellent electron transport properties due to its high electron affinity and mobility [12,13]. Although both materials belong to the fullerene family, their roles are complementary rather than redundant. PCBM primarily improves interfacial charge extraction and passivation, whereas C_{60} supports efficient carrier transport and reduces resistive losses within the ETL stack. The combination of these two materials is therefore expected to enhance the overall performance of the device.

Finally, ITO (Indium Tin Oxide) functions as the transparent conductive electrode (TCE). Its excellent electrical conductivity and optical transparency in the visible range make it ideal for allowing light into the device while conducting the generated current [14,15].

However, the device performance of Cs_2BiAgI_6-based solar cells remains limited due to inefficient charge transport and unfavorable energy band alignment. To address these challenges, designing appropriate transport layers and heterojunction architectures is essential.

In this work, a novel double-heterojunction device structure incorporating a PCBM/C_{60} bilayer electron transport layer and a CdTe hole transport layer is proposed. The device performance and energy band alignment are systematically analyzed using wxAMPS simulation to optimize the photovoltaic characteristics of the proposed structure.

By thoughtfully combining these materials, this solar cell design aims to deliver both high efficiency and improved environmental compatibility, potentially offering a superior alternative to traditional lead-based solar technologies.

2 Simulation Framework and Numerical Model

The electrical and optical performance of the perovskite solar cell was simulated using the wxAMPS (Analysis of Microelectronic and Photonic Structures) software. It is a one-dimensional device simulator widely employed for modeling multilayer photovoltaic structures. The simulator solves Poisson's equation

coupled with the continuity equations for electrons and holes under steady-state conditions, enabling accurate modeling of charge transport, recombination, and electrostatic potential distribution [16].

Simulations were conducted under AM1.5G illumination (1000 W/m^2) at a temperature of 300 K to represent standard operating conditions. The device structure was modeled as a multilayer heterojunction consisting of ITO/PCBM/C_{60}/Cs_2BiAgI_6/CdTe/Au.

For each layer, the relevant electronic parameters-bandgap energy (E_g), electron affinity (X), relative permittivity (ε), donor (N_d) and acceptor (N_a) densities, effective density of states (N_c, N_v), and carrier mobilities (μ_e, μ_h) were defined based on reported experimental data. The selected values are summarized in Table 1 [3,17–19].

The optical absorption coefficient of the absorber layer was estimated using the Tauc relation, providing a realistic description of photon absorption and carrier generation. After defining all material parameters, wxAMPS computed the steady-state solutions for potential distribution and carrier transport.

The device structure considered in the simulation is described in detail in Section 3. In the present study, thickness optimization was performed by varying one layer at a time (ETL, absorber, or HTL thickness) over a defined range, while keeping all other device parameters constant, in order to isolate the effect of each parameter on the overall device performance.

Table 1: The electric parameters sitting for the simulated Cs_2BiAgI_6 solar cell used in the wxAMPS [3,17–19].

	ITO	PCBM	C60	Cs_2BiAgI_6	CdTe
E_g (eV)	3.5	2	1.7	1.6	1.5
ε	9	3.9	4.2	6.5	9.4
X (eV)	4	3.9	3.9	3.9	3.9
N_c (cm^{-3})	2.2×10^{18}	2.5×10^{21}	8×10^{19}	1.0×10^{19}	8×10^{17}
N_v (cm^{-3})	1.8×10^{19}	2.5×10^{21}	8×10^{19}	1×10^{19}	1.8×10^{19}
M_e (cm^2/v/s)	20	0.2	8×10^{-2}	2	320
M_h (cm^2/v/s)	10	0.2	3.5×10^{-3}	2	40
N_d (cm^{-3})	1×10^{21}	2.93×10^{17}	1×10^{17}	0	0
N_a (cm^{-3})	0	0	0	1×10^{15}	2×10^{14}

3 Device Structure

In this investigation, the double heterojunction perovskite solar cell (PSC) was modeled using wxAMPS simulation software. The device structure, [ITO/PCBM/C_{60}/Cs_2BiAgI_6/CdTe/Au], is illustrated in Fig. 1. This novel structure consists of Cs_2BiAgI_6, a lead-free double perovskite, as the absorber layer. While the electron transport layer (ETL). Organic semiconductors were chosen, bilayers of PCBM and C_{60}. The p-type CdTe is used as a hole transport layer (HTL). At the same time, ITO serves as a transparent conductive oxide (TCO). This novel solar cell design builds upon previous research, aiming to combine the advantages of Cs_2BiAgI_6 and CdTe with efficient charge transport layers to achieve high power conversion efficiency and stability.

Energy Band Alignment

The energy band alignment of the proposed device is evaluated using the bandgap and electron affinity values listed in Table 1. The conduction band minimum (CBM) and valence band minimum (VBM) positions of each layer are determined using the electron affinity rule. Energy band alignment of the PSC device structure is illustrated in Fig. 2.

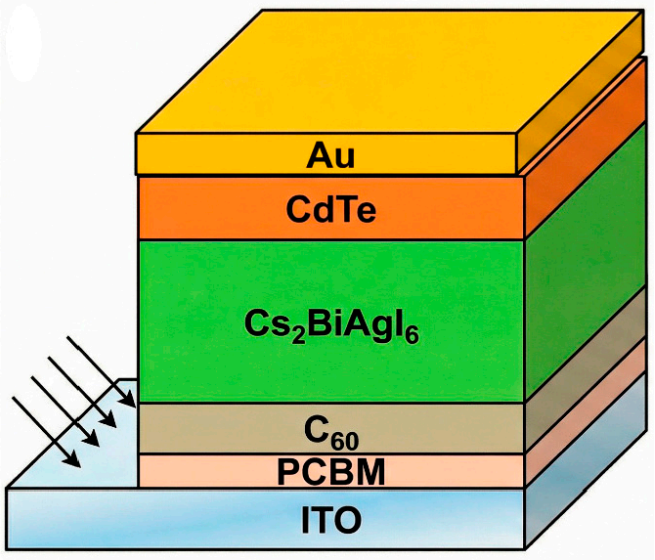

Figure 1: Schematic diagram of the simulated Cs_2BiAgI_6 solar cell structure.

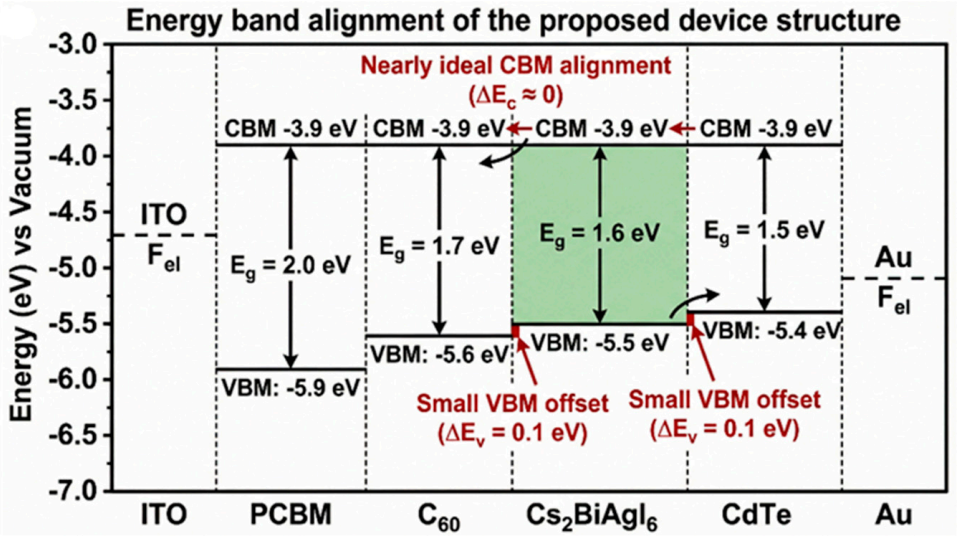

Figure 2: Energy band alignment of the proposed PSC device structure.

PCBM has E_g of about 2.0 eV and a χ of 3.9 eV, giving a CBM near −3.9 eV and a VBM around −5.9 eV. Likewise, C_{60} exhibits a E_g ~1.7 eV with the same χ value of 3.9 eV, resulting in a CBM of about −3.9 eV and a VBM near −5.6 eV. The Cs_2BiAgI_6 absorber layer has a E_g of 1.6 eV and a χ of 3.9 eV, corresponding to a CBM of about −3.9 eV and a VBM near −5.5 eV.

The conduction band alignment among PCBM, C_{60}, and Cs_2BiAgI_6 is therefore nearly ideal, with an almost-zero conduction band offset. Such a negligible offset provides a barrier-free pathway for electron extraction from the absorber to the ETL side, thereby facilitating efficient electron transport and suppressing interfacial carrier accumulation. In addition, the small valence band offset between C_{60} and Cs_2BiAgI_6 [ΔE_v = 0.1 eV] helps maintain carrier selectivity and reduces back-transfer losses.

Although CdTe is traditionally used as an absorber material on thin-film solar cell, in the present study, it is employed as a hole-transport layer due to its favorable electronic properties. It has an E_g of about 1.5 eV

and a χ of 3.9 eV. That gives a CBM near −3.9 eV and a VBM around −5.4 eV. The energy band alignment analysis reveals a small valence band offset (~0.1 eV) between Cs_2BiAgI_6 and CdTe, which enables efficient hole extraction across the interface. Moreover, the nearly flat conduction band alignment ($\Delta E_c \approx 0$) helps to block electron backflow and suppress interfacial recombination. In addition, CdTe exhibits relatively high hole mobility and p-type conductivity, which further enhances hole transport toward the back contact. These characteristics make CdTe a suitable HTL candidate in the proposed device architecture despite its conventional use as an absorber material.

Overall, the band structure of the proposed device shows favorable energy-level matching at both the ETL/absorber and absorber/HTL interfaces. The near-flat CB alignment promotes efficient electron collection through PCBM/C_{60}. Whereas the small VB offset between Cs_2BiAgI_6 and CdTe enables effective hole transport. Such a favorable band alignment is expected to reduce interfacial recombination and contribute to the enhanced photovoltaic performance of the simulated perovskite solar cell.

4 Results and Discussions

To optimize the performance of the simulated solar cell structure, it's crucial to ensure that the layer thicknesses are at their optimal value. These layer thicknesses influence the photovoltaic performance. Therefore, we investigated the effects of C_{60}-ETL, CdTe-HTL, and Cs_2BiAgI_6-absorber layer thicknesses on various solar cell performance parameters. These parameters include J_{sc}, V_{oc}, FF, and Eff.

4.1 The Effect of ETL Thickness on Electrical Properties

The study examined how the thickness of the ETL layer affects device performance, with the ITO layer fixed at 50 nm, the absorber layer at 2 μm, and both PCBM and CdTe at 200 nm. The ETL thickness varied from 100 nm to 600 nm in 100 nm steps.

Fig. 3 shows the obtained solar cell performance as a function of the C_{60}-electron transport layer (ETL) thickness. As the thickness increases from 100–600 nm, we observe a modest rise in the (J_{sc}) value, shifting from 23.74 to 23.81 mA/cm^2. In contrast, the (V_{oc}) value remains relatively unchanged, as illustrated in Fig. 3a,b. From a carrier-transport perspective, the C_{60} layer facilitates selective electron extraction while blocking holes due to its favorable conduction-band alignment with the absorber. Increasing the ETL thickness can improve interfacial coverage and reduce defect-assisted recombination at the absorber/ETL interface. This leads to a marginal improvement in electron collection efficiency, which explains the slight increase in Jsc. However, since the conduction band alignment is already nearly ideal ($\Delta E_c \approx 0$), further increases in ETL thickness do not significantly enhance charge separation, resulting in minimal variation in V_{oc}. At the same time, increasing ETL thickness introduces additional series resistance, which limits further performance gains. This behavior is consistent with drift-diffusion transport models, where carrier extraction efficiency depends on both interface quality and layer resistance.

Furthermore, the fill factor (FF) increases from 86.06% to 86.19% as the thickness increases. Additionally, the rise in ETL thickness affects the efficiency (Eff), which varies from 22.10% to 22.22%, as shown in Fig. 3c,d.

Efficiency is a function of J_{sc}, V_{oc}, and FF. The slight increases in J_{sc} and FF, combined with stable V_{oc}, lead to a slight improvement in overall efficiency. This indicates that moderate thickening of the C_{60}-ETL enhances performance, but beyond a certain point, gains plateau or may even reverse due to resistive losses. Thicker ETLs can improve quality and charge extraction, but at the cost of increased series resistance [20–22]. Performance benefits are modest, suggesting the system is nearing an optimal ETL thickness. Further thickening could eventually harm performance.

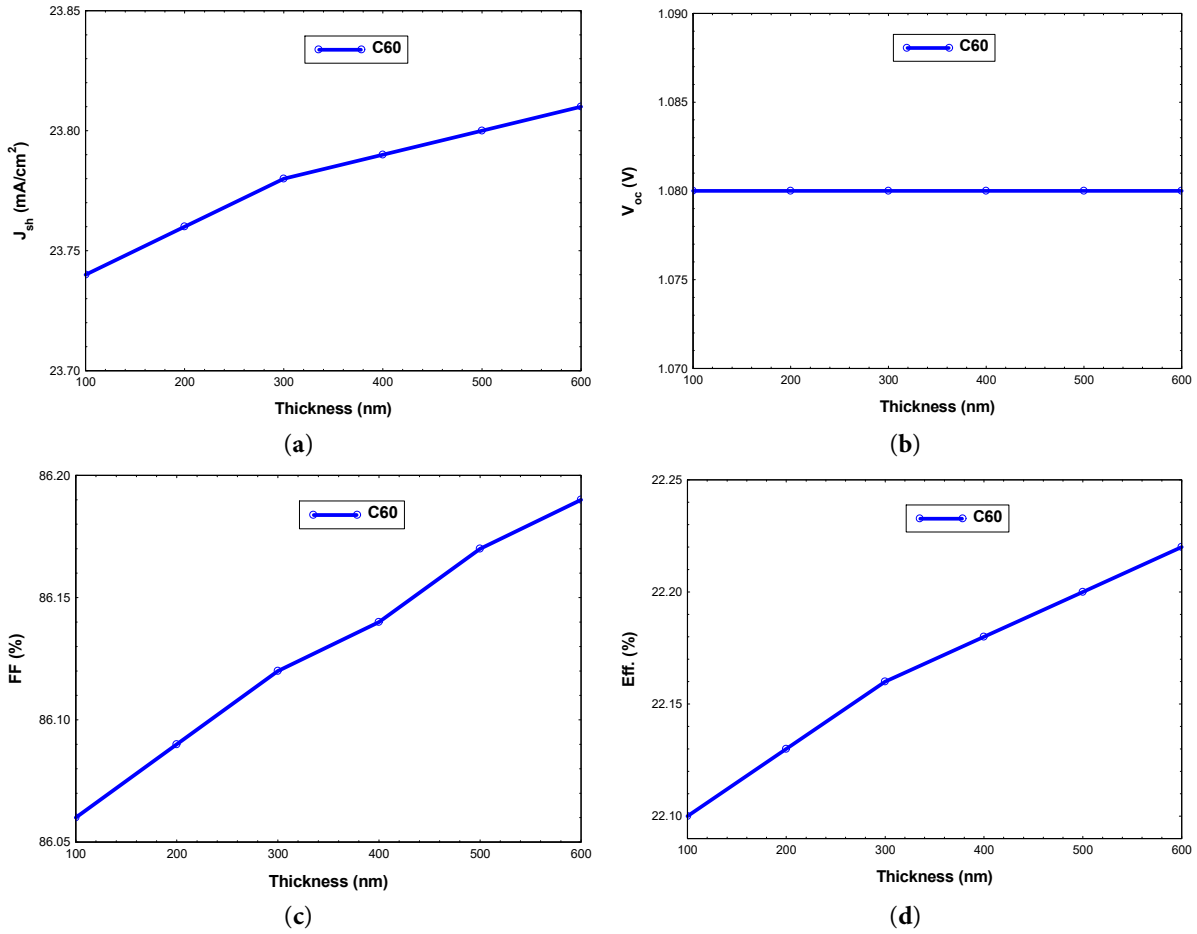

Figure 3: Effect of C_{60} (ETL) thickness on the photovoltaic performance of the proposed device. (**a**) Short-circuit current density (J_{sc}), (**b**) open-circuit voltage (V_{oc}), (**c**) fill factor (FF), and (**d**) power conversion efficiency (Eff). The *x*-axis represents the C_{60} thickness (nm), and the *y*-axis represents the corresponding electrical parameter. All other device parameters were kept constant during the simulation.

4.2 The Effect of HTL Thickness on Electrical Properties

The study investigated how HTL layer thickness influences device performance, with the ITO fixed at 50 nm, the absorber layer at 2 μm, and both PCBM and C_{60} at 200 nm. The HTL thickness was varied from 100 nm to 600 nm, in 100 nm increments.

Fig. 4 illustrates the effect of varying the thickness of the CdTe hole transport layer (HTL) from 100 to 600 nm on solar cell performance. The J_{sc} remains constant at 23.76 mA/cm^2 throughout this range, as observed in Fig. 4a. This indicates that changes in CdTe-HTL thickness have minimal impact on photon absorption or charge carrier generation. This makes sense, as the HTL primarily affects hole transport rather than light absorption, which is dominated by the absorber layer. From a carrier dynamics perspective, the primary role of the HTL is to facilitate efficient hole extraction and transport while blocking electrons. The small valence band offset (~0.1 eV) between Cs_2BiAgI_6 and CdTe enables efficient hole transfer across the interface, minimizing energy barriers for hole transport. As the HTL thickness increases, a slight improvement in V_{oc} is observed, as shown in Fig. 4b. This behavior can be attributed to reduced interfacial recombination and improved hole selectivity, which enhances the quasi-Fermi level splitting. Additionally,

a thicker HTL can improve the built-in electric field distribution near the back contact, contributing to more efficient carrier extraction.

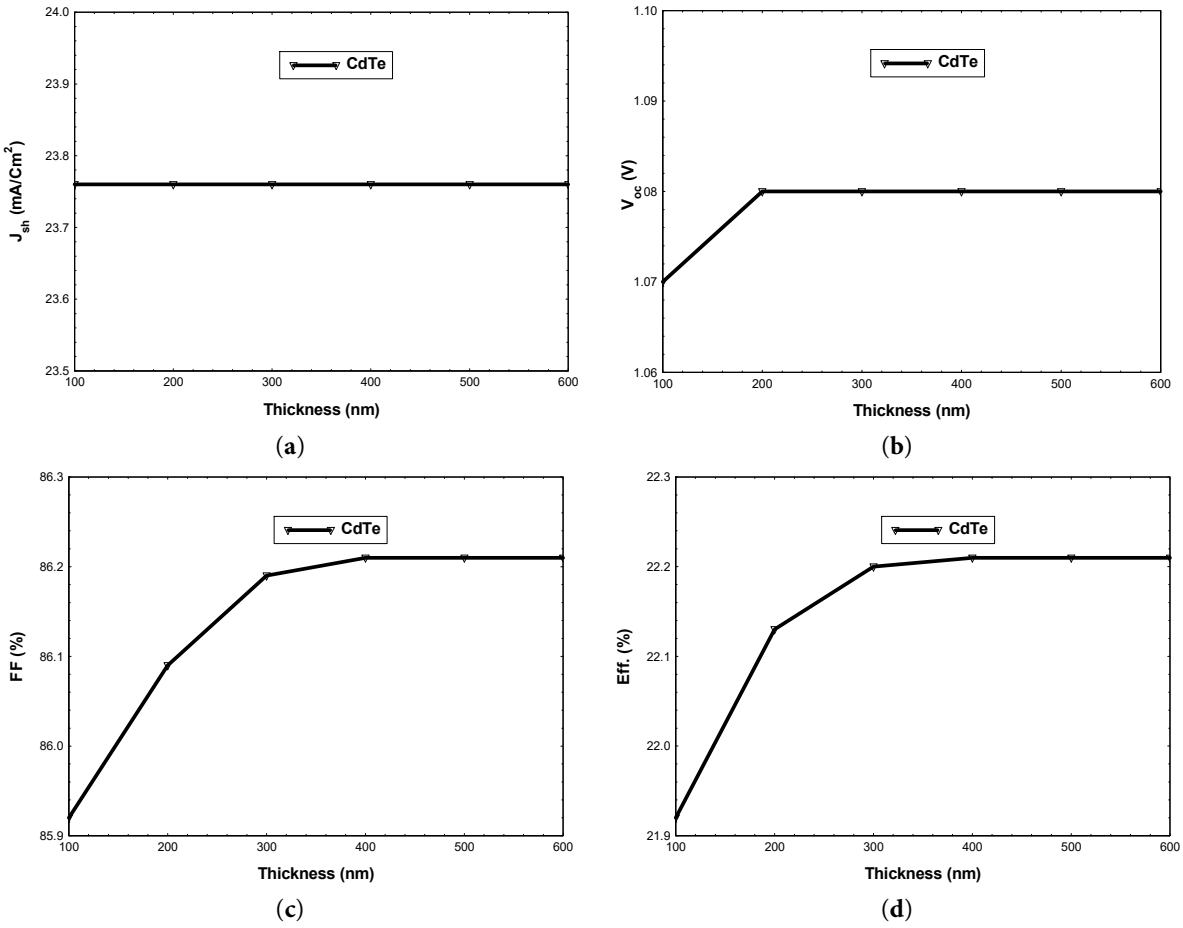

Figure 4: Effect of CdTe (HTL) thickness on the photovoltaic performance of the proposed device. (**a**) Short-circuit current density (J_{sc}), (**b**) open-circuit voltage (V_{oc}), (**c**) fill factor (FF), and (**d**) power conversion efficiency (Eff). The *x*-axis represents the CdTe thickness (nm), and the *y*-axis represents the corresponding electrical parameter. All other device parameters were kept constant during the simulation.

The FF improves slightly from 85.92% to 86.21%. As a result, the Eff experiences a minor enhancement, increasing from 21.90% to 22.21%, as depicted in Fig. 4c,d. The results indicate that HTL thickness optimization primarily influences recombination dynamics and carrier selectivity rather than photogeneration, leading to gradual improvements in V_{oc}, FF, and overall efficiency.

4.3 The Effect of the Absorber Layer Thickness on Electrical Properties

The study examined how the thickness of the absorber layer affects device performance, with the ITO fixed at 50 nm and both PCBM and C_{60} at 200 nm, as well as the CdTe at 200 nm. The absorber layer thickness was varied from 100 nm to 2 μm, in 100 nm steps.

Fig. 5 presents the impact of varying the thickness of the Cs_2BiAgI_6 absorber layer, ranging from 100 nm to 2 μm, on the performance metrics of the solar cell. As shown in Fig. 5a, the J_{sc} initially increases from 24.97 mA/cm^2 to a peak of 25.32 mA/cm^2 at thicknesses of 300–400 nm. Beyond this point, J_{sc} declines, reaching 23.43 mA/cm^2 at 900 nm, followed by a slight recovery to 23.76 mA/cm^2 at greater thicknesses.

The initial increase in J_{sc} suggests improved light absorption due to greater material volume. However, beyond a certain thickness of 400 nm increased recombination and poor charge transport likely reduce carrier collection, resulting in a drop in J_{sc}.

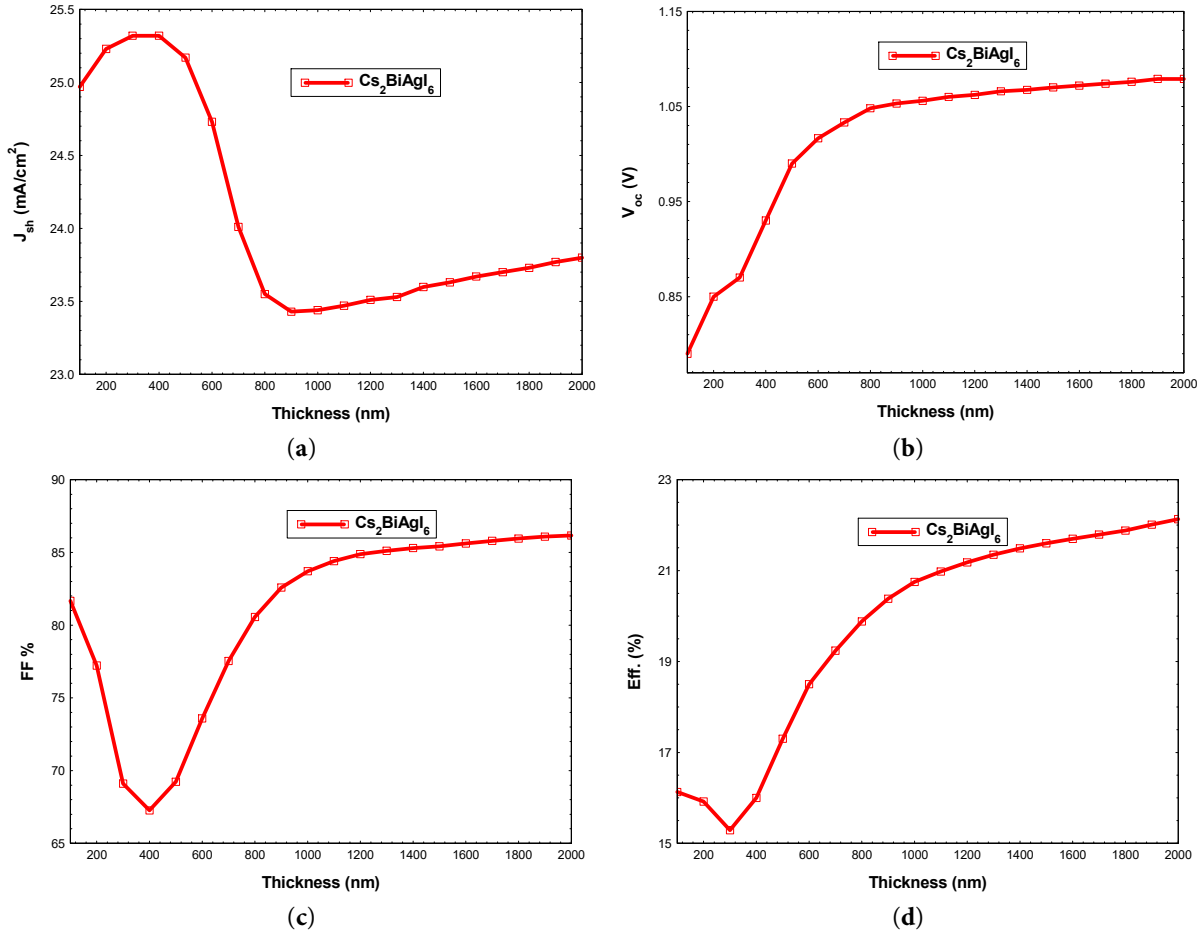

Figure 5: Effect of Cs_2BiAgI_6—absorber layer thickness on the photovoltaic performance of the proposed device. (**a**) Short-circuit current density (J_{sc}), (**b**) open-circuit voltage (V_{oc}), (**c**) fill factor (FF), and (**d**) power conversion efficiency (Eff). The *x*-axis represents the Cs_2BiAgI_6 thickness (nm), and the *y*-axis represents the corresponding electrical parameter. All other device parameters were kept constant during the simulation.

Fig. 5b illustrates that the V_{oc} consistently increases with thickness, starting at 0.79 V and reaching up to 1.08 V. This behavior may be associated with improved junction operation and reduced effective recombination losses under the optimized device configuration.

Fig. 5c shows that the FF initially drops from 81.67% to a minimum of 67.27% at 400 nm, but then improves to a peak of 86.09% at 2 μm. Consequently, the power conversion efficiency (Eff), shown in Fig. 5d, follows a similar trend, dropping from 16.13% to a minimum of 15.29% at 300 nm before increasing to a maximum of 22.13% at 2 μm thickness. What emerges here is a fairly typical trade-off. Increasing the absorber thickness does help with light harvesting, but it also starts to push against the limits of transport charge. In the case of Cs_2BiAgI_6, this balance becomes even more sensitive because of its indirect bandgap and only moderate absorption.

So, the improvement at larger thickness is not really about the material suddenly performing better optically. It has more to do with how the device is put together. With favorable band alignment and efficient transport layers. It enables improved carrier extraction and reduced recombination, ultimately leading to enhanced overall device efficiency. For that reason, the peak efficiency observed at 2 μm should be understood as the outcome of overall structural optimization. It does not provide evidence that Cs_2BiAgI_6 intrinsically behaves like a highly absorbing direct-bandgap perovskite.

From a practical perspective, achieving such thickness may introduce challenges, including increased bulk defect density and enhanced recombination losses during fabrication. Therefore, the results obtained in this work should be considered as an optimized theoretical scenario. Future experimental studies may explore alternative strategies, such as light trapping or optical enhancement techniques, to achieve similar performance with reduced absorber thickness.

4.4 Performance of the Optimized Device Configuration

Based on the simulation results discussed in the previous sections, the optimal thicknesses of the individual layers in the solar cell structure were determined to maximize device performance. The finalized configuration includes an indium tin oxide (ITO) layer with a thickness of 50 nm, a PCBM electron-transport layer of 600 nm, a C_{60} interlayer also at 600 nm, a Cs_2BiAgI_6 perovskite absorber layer of 2 μm, and a CdTe hole transport layer of 600 nm. This carefully engineered layer structure balances efficient light absorption, charge carrier separation, and transport, resulting in high overall device performance.

Fig. 6 presents the current density-voltage (J-V) characteristics of the optimized solar cell under standard illumination conditions. Key performance indicators obtained from the simulation include a J_{sc} of 23.23 mA/cm^2, a V_{oc} of 1.08 V, a R_s of 0.25 Ω·cm^2, and a R_{sh} of 7123 Ω·cm^2. The device also exhibited a high FF of 86.35% and an Eff of 22.33%. These values indicate strong photovoltaic performance and efficient charge carrier dynamics within the cell.

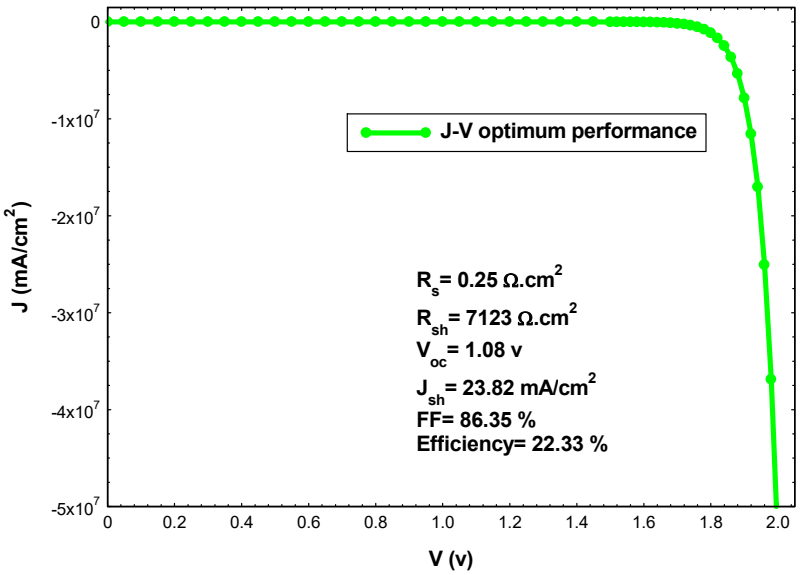

Figure 6: The current density-voltage (J-V) characteristics of the optimum solar cell performance.

The use of Cs_2BiAgI_6 as a lead-free double perovskite absorber offers significant advantages in terms of environmental safety and material stability compared to conventional lead-based perovskites. Its optimal thickness (2 μm) ensures sufficient photon absorption across the solar spectrum, while the PCBM and C_{60}

layers effectively facilitate electron transport and reduce interfacial recombination. CdTe, widely recognized for its high hole mobility, serves as an efficient hole-transport layer, thereby further enhancing carrier extraction. The low series resistance and high shunt resistance values indicate minimal resistive losses and leakage currents, which contribute to the high fill factor observed. Altogether, these results highlight the potential of the proposed structure for high-efficiency, lead-free solar cells, demonstrating both strong performance metrics and environmentally sustainable material choices.

Fig. 7 illustrates the quantum efficiency (QE) spectrum of the optimized solar cell under standard operating conditions. The QE remains consistently high across a broad wavelength range, demonstrating strong photon-to-electron conversion efficiency. Specifically, in the spectral range of 200–733 nm, the device exhibits a nearly constant quantum efficiency of approximately 96%, indicating effective light absorption and carrier collection in this region. Beyond 733 nm, the QE sharply declines and reaches zero at around 788 nm, marking the cutoff wavelength beyond which the device no longer responds to incident photons.

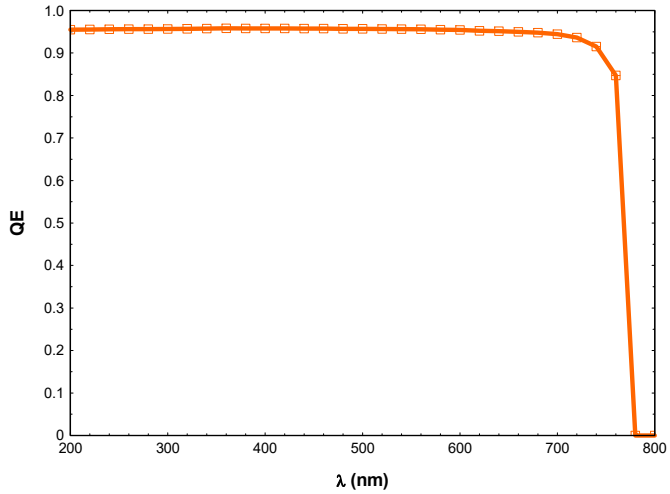

Figure 7: The quantum efficiency for the optimum solar cell performance.

The high and steady quantum efficiency observed between 200 and 733 nm confirms the excellent optical absorption and charge carrier extraction capabilities of the active layers, particularly the Cs_2BiAgI_6 absorber in combination with the transport layers. The strong QE in the visible and near-UV region implies that most photons in this range are successfully converted into electrical current, which significantly contributes to the high J_{sc} observed.

The abrupt decline in QE after 733 nm dropping to zero by 778 nm, suggests that photons with wavelengths longer than this threshold do not possess sufficient energy to overcome the bandgap of the absorber material. This behavior aligns with the expected spectral response of perovskite-based absorbers, where the absorption edge is determined by the material's bandgap. The sharp cutoff indicates minimal sub-bandgap absorption or parasitic losses, which is favorable for efficient device operation. Overall, the QE spectrum reinforces the effectiveness of the material selection and layer design in maximizing light harvesting and charge collection, particularly within the high-intensity portion of the solar spectrum.

One of the inherent limitations of Cs_2BiAgI_6 is its relatively weak absorption in the near-infrared (NIR) region, primarily due to its indirect bandgap nature. As a result, a significant portion of the solar spectrum remains unutilized, which limits the achievable photocurrent density.

To address this limitation, advanced photonic strategies, such as the incorporation of upconversion materials, have been proposed in recent studies [23]. Rare-earth-doped phosphors, such as $NaYF_4:Yb^{3+}$,

Er^{3+}, and $NaYF_4$:Yb^{3+}, Tm^{3+}, are capable of converting low-energy NIR photons into higher-energy visible photons through nonlinear optical processes. These converted photons can then be effectively absorbed by the perovskite layer, thereby enhancing the device's spectral response.

Although the present study is based on numerical simulation and does not explicitly include upconversion layers, the integration of such materials represents a promising direction for future work to overcome the intrinsic absorption limitations of Cs_2BiAgI_6 and further improve device efficiency.

The simulated energy band diagram of the optimized PSC is shown in Fig. 8. It includes the conduction band edge E_c, valence band edge E_v, and the quasi-Fermi levels for electrons E_{fn} and holes E_{fp} along the device thickness.

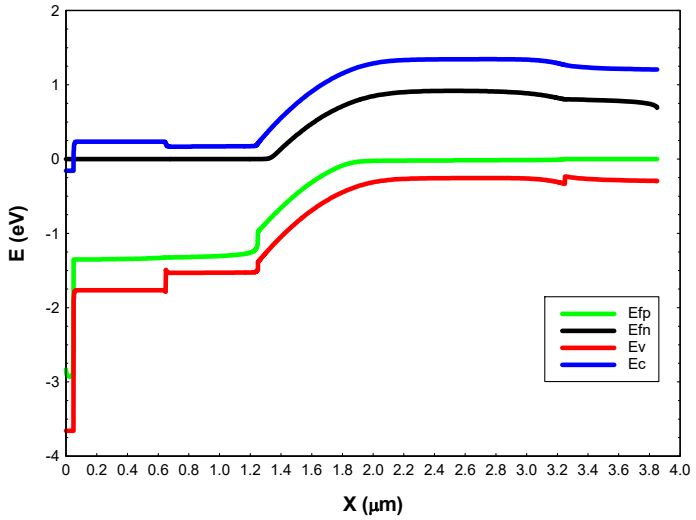

Figure 8: Simulated energy band diagram of the proposed PSC structure showing the E_c, E_v, E_{fn}, and E_{fp} along the device thickness.

The band diagram reveals clear discontinuities at the material interfaces, confirming the formation of a multilayer heterojunction structure. At the front side of the device, the conduction band alignment between the ETL layers (PCBM/C_{60}) and the Cs_2BiAgI_6 absorber provides a favorable pathway for electron transport toward the front contact. The small conduction band offset reduces potential barriers for electron extraction and minimizes interfacial recombination losses.

Within the Cs_2BiAgI_6 absorber layer, noticeable band bending is observed, indicating the presence of a built-in electric field across the junction. This internal electric field facilitates the separation of photogenerated carriers, driving electrons toward the ETL side while holes move toward the CdTe layer.

At the absorber/HTL interface, the valence band alignment between Cs_2BiAgI_6 and CdTe enables efficient hole extraction toward the back contact. Meanwhile, the conduction band discontinuity acts as an electron-blocking barrier, suppressing electron back transfer and reducing recombination at the rear interface.

Furthermore, the separation between the electron and hole quasi-Fermi levels inside the absorber confirms effective carrier separation under illumination conditions. Overall, the simulated band structure demonstrates that the proposed device architecture provides favorable energy-level alignment for efficient charge transport and enhanced photovoltaic performance.

The quasi-Fermi level splitting observed in the absorber region corresponds to the photovoltage generated in the device and reflects the capability of the proposed structure to maintain efficient carrier separation.

As shown in Table 2, previously reported different double perovskite solar cells generally exhibit relatively low efficiencies due to intrinsic limitations such as indirect bandgap characteristics and weak absorption. In contrast, the proposed device achieves a significantly higher efficiency of 22.33%.

Table 2: Comparison of reported different double perovskite solar cell performance.

Reference	Structure	Method	Efficiency
Wu et al. [24]	ITO/SnO_2/$Cs_2AgBiBr_6$/P_3HT/Au	Experimental	1.44%
Mustafa et al. [25]	Cs_2BiAgI_6-based devices	SCAPS simulation	21.2%
Hossain et al. [3]	Cs_2BiAgI_6-based device	SCAPS simulation	~14.4–21.5%
Current study	PCBM/C60/Cs_2BiAgI_6/CdTe	wxAMPS simulation	22.33%

This improvement is primarily attributed to the optimized double-heterojunction architecture, which enhances charge separation and reduces recombination losses. The incorporation of a bilayer ETL (PCBM/C_{60}) improves electron extraction and transport, while the CdTe layer provides efficient hole extraction due to favorable band alignment. Additionally, absorber thickness optimization plays a key role in improving overall device performance. These results demonstrate the effectiveness of the proposed design strategy in overcoming the limitations of lead-free double perovskite materials.

5 Conclusion

This work presents a comprehensive simulation-based optimization of a lead-free double perovskite solar cell using Cs_2BiAgI_6 as the absorber material. The study focused on tuning the thicknesses of the transport and absorber layers to identify the configuration that yields maximum device efficiency. Results indicate that increasing the thickness of the C_{60}-ETL and CdTe-HTL to 600 nm yields modest gains in efficiency, attributed to enhanced charge transport and reduced recombination. More significantly, optimizing the absorber layer thickness to 2 μm enhances photon absorption without incurring excessive recombination losses, thereby substantially improving the overall performance.

The finalized device configuration demonstrated excellent electrical characteristics, including a high fill factor and an efficiency of 22.33%. The quantum efficiency analysis confirmed that the cell maintains high responsiveness across the majority of the solar spectrum, with a sharp cutoff at 778 nm, indicative of well-defined optical properties and effective energy conversion. Notably, the use of a lead-free double perovskite not only achieves competitive efficiency but also addresses the environmental concerns associated with lead-based perovskite solar cells. These findings open the door for the development of high-efficiency, environmentally friendly photovoltaic technologies.

Acknowledgement: The author acknowledges the valuable discussions and feedback provided by colleagues during the course of this work. AI tools were used solely to improve the clarity and readability of the manuscript. All scientific content, analysis, and conclusions are the responsibility of the author.

Funding Statement: The author received no specific funding for this study.

Availability of Data and Materials: The data supporting the findings of this study are available from the corresponding author upon reasonable request. No publicly available datasets were generated or analyzed in this study.

Ethics Approval: Not applicable.

Conflicts of Interest: The author declares no conflicts of interest.

References

1. Liu X, Zhao W, Cui H, Xie YA, Wang Y, Xu T, et al. Organic–inorganic halide perovskite based solar cells–revolutionary progress in photovoltaics. Inorg Chem Front. 2015;2(4):315–35. [CrossRef].
2. He R, Ren S, Chen C, Yi Z, Luo Y, Lai H, et al. Wide-bandgap organic–inorganic hybrid and all-inorganic perovskite solar cells and their application in all-perovskite tandem solar cells. Energy Environ Sci. 2021;14(11):5723–59. [CrossRef].
3. Hossain MK, Arnab AA, Das RC, Hossain KM, Rubel MHK, Rahman MF, et al. Combined DFT, SCAPS-1D, and wxAMPS frameworks for design optimization of efficient Cs_2BiAgI_6-based perovskite solar cells with different charge transport layers. RSC Adv. 2022;12(54):35002–25. [CrossRef].
4. Hossain MK, Samajdar DP, Das RC, Arnab AA, Rahman MF, Rubel MHK, et al. Design and simulation of Cs_2BiAgI_6 double perovskite solar cells with different electron transport layers for efficiency enhancement. Energy Fuels. 2023;37(5):3957–79. [CrossRef].
5. Kumar A, Shkir M, Somaily HH, Singh KL, Choudhary BC, Tripathi SK. A simple, low-cost modified drop-casting method to develop high-quality $CH_3NH_3PbI_3$ perovskite thin films. Phys B Condens Matter. 2022;630:413678. [CrossRef].
6. Romeo A, Artegiani E. CdTe-based thin film solar cells: Past, present and future. Energies. 2021;14(6):1684. [CrossRef].
7. Al Suny A, Noor T, Hossain MH, Sheikh AFMAU, Chowdhury MH. Broadband absorption in cadmium telluride thin-film solar cells via composite light trapping techniques. arXiv:2502.20539. 2025.
8. Scarpulla MA, McCandless B, Phillips AB, Yan Y, Heben MJ, Wolden C, et al. CdTe-based thin film photovoltaics: Recent advances, current challenges and future prospects. Sol Energy Mater Sol Cells. 2023;255:112289. [CrossRef].
9. Korotcenkov G. Cd- and Zn-based wide band gap II–VI semiconductors. In: Handbook of II–VI semiconductor-based sensors and radiation detectors: Volume 1, materials and technology. Berlin/Heidelberg, Germany: Springer; 2023. p. 21–65. [CrossRef].
10. Del Sordo S, Abbene L, Caroli E, Mancini AM, Zappettini A, Ubertini P. Progress in the development of CdTe and CdZnTe semiconductor radiation detectors for astrophysical and medical applications. Sensors. 2009;9(5):3491–526. [CrossRef].
11. Liu Q, Zhang X, Abdalla LB, Zunger A. Transforming common III–V and II–VI semiconductor compounds into topological heterostructures: The case of CdTe/InSb superlattices. Adv Funct Mater. 2016;26(19):3259–67. [CrossRef].
12. Zhu Z, Xue Q, He H, Jiang K, Hu Z, Bai Y, et al. A PCBM electron transport layer containing small amounts of dual polymer additives that enables enhanced perovskite solar cell performance. Adv Sci. 2016;3(9):1500353. [CrossRef].
13. Mumyatov AV, Troshin PA. A review on fullerene derivatives with reduced electron affinity as acceptor materials for organic solar cells. Energies. 2023;16(4):1924. [CrossRef].
14. Ali AH, Shuhaimi A, Hassan Z. Structural, optical and electrical characterization of ITO, ITO/Ag and ITO/Ni transparent conductive electrodes. Appl Surf Sci. 2014;288:599–603. [CrossRef].
15. Sharma S, Shriwastava S, Kumar S, Bhatt K, Tripathi CC. Alternative transparent conducting electrode materials for flexible optoelectronic devices. Opto Electron Rev. 2018;26(3):223–35. [CrossRef].
16. Liu Y, Heinzel D, Rockett A. A new solar cell simulator: wxAMPS. In: Proceedings of the 2011 37th IEEE Photovoltaic Specialists Conference; 2011 Jun 19–24; Seattle, WA, USA. [CrossRef].
17. Gong J. Simulation of steady-state characteristics of heterojunction perovskite solar cells in wxAMPS. Optik. 2021;232:166382. [CrossRef].
18. Hashmi G, Hossain MS, Rashid MJ. Simulation of CdTe, CIGS and CZTS solar cells using wxAMPS software. Res Sq. 2021. [CrossRef].
19. Banerjee S. High efficiency CdTe/CdS thin film solar cell. Int J Eng Res Technol. 2015;4(9):700–3.
20. Zhang L, Lu W, Ding F, Jin R, Wang Q. Ultrathin ALD-SnO_2 interlayer for performance enhancement of inverted perovskite solar cells. Mater Today Commun. 2025;46:112921. [CrossRef].

21. Bouziane A, El Ghazi H, En-nadir R, Belaid W, Abboudi H, Sali A. Effects of doping, transport layer thickness, and composition on the performance of mixed halide perovskite single-junction solar cells. J Electron Mater. 2025;54(9):7296–307. [CrossRef].
22. Mukametkali TM, Ilyassov BR, Aimukhanov AK, Serikov TM, Baltabekov AS, Aldasheva LS, et al. Effect of the TiO_2 electron transport layer thickness on charge transfer processes in perovskite solar cells. Phys B Condens Matter. 2023;659:414784. [CrossRef].
23. Kumar A, Kant Tripathi S, Deshmukh AD. Dual mode emission in NaYF4:Yb Er nanorods for photovoltaics application. Adv Mater Lett. 2015;6(8):701–5. [CrossRef].
24. Wu C, Zhang Q, Liu Y, Luo W, Guo X, Huang Z, et al. The dawn of lead-free perovskite solar cell: Highly stable double perovskite $Cs_2AgBiBr_6$ film. Adv Sci. 2018;5(3):1700759. [CrossRef].
25. Mustafa GM, Akhtar MS, Sabir U, Almaymoni NK, El-Fattah WA, Mnif W, et al. Mechanistic insights into performance limitation and optimization of lead-free double perovskite $Cs_2BiAgI6$ solar cells. J Sol Gel Sci Technol. 2026;117(2):45. [CrossRef].